Solvent induced ^{1}H NMR chemical shifts of annulenes

Swrangsi Goyary[a], Manash Jyoti Sarmah[a], Himangshu Prabal Goswami[*a], and Nilamoni Nath[*a]

[a]Department of Chemistry, Gauhati University, Guwahati-781014

To whom the correspondence is to be addressed:

hpg@gauhati.ac.in

nnath@gauhati.ac.in

Abstract

We investigate the effect of solvent polarity on the ^{1}H NMR chemical shifts of [n]annulenes (n = 12, 18, and 30) using density functional theory and corroborate the computational results with Onsager's reaction field theory. We observe that there is a complete deshielding of the proton NMR chemical shifts for the outer protons and these shifts depend linearly on the dielectric function of the solvents reaction field for certain annulenes (n = 12 and 30). For the asymmetric C_2 structure of [18]annulene, the inner protons are observed to vary nonlinearly with the function of solvent dielectrics due to the influence of the asymmetry parameter "*C*", which generates an anisotropic environment inside the annulene ring cavity.

Introduction

Proton NMR chemical shifts, being very sensitive to molecular interactions, respond remarkably to the conformational changes in the sample. NMR spectroscopy demonstrates the specificity of aromatic solvents, with the compound proton signals being displaced upfield in aromatic solvents compared to the case when these are in magnetically isotropic solvents. As a commonly observed phenomenon, ^{1}H NMR chemical shifts of polar compounds in aromatic solvents move downfield in comparison to magnetically isotropic solvents [1], usually called the aromatic solvent induced shift (SIS). SIS depends on both the solute site properties and the solvent parameters [2,3]. The sign and magnitude of NMR chemical shifts are known to vary when the internal reference compounds and solvents are changed, especially with aromatic systems [4]. In macrocyclic systems with NH- functional groups, each proton signal is shifted upfield upon changing the solvent from toluene to cyclohexane [5]. In chloroform, shifts of about 1 ppm are seen upon changing the solvent from cyclohexane to benzene [6]. A plethora of experimental and theoretical research has already been carried out on such solvent induced changes in NMR spectroscopy [7-11]. These chemical shifts have been attributed to solute-solvent clustering or the formation of solvation spheres which gives rise to solvated solute sites or cavities where the electrical activity is rich and is called the *reaction field* [3,12]. Hydrogen bonding, anisotropy in the solvent molecules, weak van der Waals interactions, unspecific shielding effects such as intrasolvent or solvent-solute $\pi \rightarrow \pi$ weak interactions [13,14] also play a role. Such SIS became a tool in proton NMR for investigating kinetic parameters [15,16] other observables like optical responses [17], lifetime of excited states [18] as well as chemical resonances [19]. At a time, SIS was an interesting technique that commanded a potential for the quantitative prediction of conformers required to design new materials or drugs [2]. However, with the advent of high-end NMR technologies, studies on SIS on structural characterization dramatically reduced [2,13]. On the theoretical front, a select few theories developed in the mid of the twentieth century are popular in the literature [2,3,8,10,20]. However, none of these microscopic in nature and each popular theory has its own drawback. With a motive to shed some light into the fundamental understanding of SIS, recently, SIS as a function of relative permittivitys (ε) of solvents was studied in alanine dipeptides [9], pyridinium iodide [21], and in the nitrogens of 1-methylazoles [7]. It has also been reported that SIS of pyridinium ring protons decrease linearly with the increase in solvent polarity [21]. Recently, SIS due to its experimental simplicity, has also been used to measure water content in organic solvents [22] and resolve crowded ^{1}H NMR signals of drug molecules [23], where

changing the polarity of the solvent led to well separated peaks. However, there exist no reports on the quantitative description of the SIS's variation curves with various solvents.

The intent of this paper is to investigate SIS as a function of solvent polarity in the ^{1}H NMR spectra of annulenes. We choose annulenes because different symmetry structures have been proposed over the years [24-26], e.g. the highly delocalized D_{6h} structure of [18]annulene deduced from the X-ray data or electron correlated geometries are debatable [24,25]. The chemical shifts calculated from the D_{6h} [18]annulene X-ray structure do not agree well with the experimental measured chemical shifts [26]. Moreover, a C_2 symmetric [18]annulene has been reported to match well with experimental NMR studies. Such discrepancies dictate the necessity of extended studies. As long as the structures does not deviate much from planarity, the magnetic properties of [4n + 2] and [4n]annulenes remain distinct. In the NMR spectra, the outer (inner) protons of a [4n + 2]annulene are found to be deshielded (shielded) while a [4n]annulenes outer (inner) protons are shielded (deshielded). These effects can be attributed to diatropic (for [4n+2]) and paratropic (for [4n]) ring currents which in turn arises from cyclic π-electron delocalization [27] . It is well known that NMR shielding tensors are influenced by rovibratory effects (vibratory motion) while the translation motion can be safely ignored [28]. This effect leads to an experimental NMR spectrum reflecting average shielding properties from vibrating and rotating molecules. However, majority of routine DFT based NMR calculations use only stationary structure corresponding to the energy minima without accounting for vibratory motion [28]. Fortunately, for computed ^{1}H NMR shifts, errors due to rovibratory effects are mostly systematic and typically small due to cancellation of errors [29-31]. There is a report on molecular dynamic simulation to estimate the chemical shift contribution from rovibratory motions but is difficult to execute being computationally expensive even for a simple molecule [28]. It has been shown that the ^{1}H NMR shifts of simulated dynamic D_{6h} structure of [18]annulene is in good agreement with experimental data while the dynamic C_2 structure exhibits somewhat disagrees [32]. Since estimation of rovibratory effect is very time consuming and expensive even for a small molecule [33] and since the chemical shifts of large systems such as natural products can be satisfactorily reproduced using stationary geometries [34,35], we choose a DFT approach that allows calculation of stationary geometries. This is quite common in majority of chemical shift applications, in other systems such as organic and natural product structure determination [34,36], inorganic materials [37], coordination chemistry [38,39], and NMR-crystallography [40,41].

In this work, we consider aromatic [18]annulene, [30]annulene and an antiaromatic [12]annulene to draw a narrative of computationally evaluated SIS and its dependence on solvent polarity (the dielectric constant, ε). We analyze the effect on the proton NMR chemical shifts of protons with increasing value of ε by considering a range of polar and nonpolar solvents (starting from apolar n-hexane to highly polar DMSO). We further corroborate the results with the reaction field theory developed by Onsager and modified by few others [10,12]. We start by the computationally optimizing each annulene in 15 different solvents from which we calculate the ^{1}H NMR spectra for the inner and outer annulenic protons. From the next section onwards, we present the computational details followed by computational results and theoretical corroboration of the results with the reaction field theory.

Computational details

We start our study by employing hybrid functionals to optimize the manually drawn [n]annulenes using Gaussian 16 [42]. The Integral Equation Formalism Polarizable Continuum model (IEFPCM), solvent model is used to separately compute each annulene's implicit solvation [43]. The geometries of the different annulenes are optimized either at B3LYP/6-311+G(d,p) or BHandHLYP/6-311+G(d,p) level of theory in gas phase and 15 other polar and non-polar solvents. The optimized geometries are then utilized to calculate the absolute shielding constants using Gauge-Independent Atomic Orbital (GIAO) method [44] at B3LYP/6-311+G(d,p) level in both gas and solution phase. The ^{1}H NMR chemical shifts for the inner (outer) protons, $\delta_i(\delta_o)$, are evaluated by subtracting the shielding constant values of the annulenes from the δ value of TMS. The relative energies of the different annulene structures are tabulated in the supporting information (Tables S1-S5). For the C_1 structure of [12]annulene and C_2 structure of [18]annulene, ^{1}H NMR chemical shifts are computed using BHandHLYP/6-311+G(d,p) geometry. For D_{6h} structure of [30]annulene, B3LYP/6-311+G(d,p) geometry is used to compute the ^{1}H NMR chemical shifts. The reasons of using different functionals are discussed later in the paper. For comparison, we demonstrate the use of various functionals for optimization and same functional to predict the ^{1}H NMR chemical shifts of [12]annulene (C_1) [18]annulene (C_2, D_{6h} and D_{3h}) and [30]annulene (D_{6h}). The data is provided in the supporting information (Tables S5-S9).

Results from the computational parameters

We now focus on the ^{1}H NMR chemical shift values that are evaluated via the GIAO method for the optimized [n]annulenes. Using the IEFPCM solvent model, we incorporates changes in the electronic charge distribution beyond the annulenic molecular cavity under consideration [45]. We optimize the highly symmetric structures of [30]annulene using the B3LYP functional since it produces less number of imaginary frequency values (BHandHLYP produces more number of imaginary frequency values (Table S5)). For the optimization of low symmetric structures of [12]- and [18]annulene, we use the BhandHLYP/6-311+G(d,p) level of theory. Additionally, the ^{1}H NMR chemical shift values at this level are remarkably close to the experimental chemical shift data [46-48] compared to the computation done with the B3LYP/6-311+G(d,p) level of theory (Tables S6-S7). For the lower symmetric structures, use of the hybrid functional is more promising because it provides a balance between the overestimation and underestimation of the degree of delocalization and generates an intermediate geometry [26]. Additionally, the relative energies of all the optimized structures are provided in Table 1. The manually drawn line structures and DFT optimized ball and bond type three dimensional (3D) structures are shown in Fig. 1. The number of imaginary frequencies of C_1 [12]-, C_2 [18]- and D_{6h} [30]annulenes are listed in Table 1. For both the [12]annulene C_1 structure, and [18]annulene C_2 structure, we do not observe any imaginary frequencies, indicating stable optimized structures (zero saddle point). The D_{6h} structure of [30]annulene has a single imaginary mode of frequency at -506 cm^{-1} indicating a transition state with a first-order saddle point, which is close to the reported mode of imaginary frequency of -461 cm^{-1}. This imaginary frequency corresponds to the B_{2u} mode of vibration in the D_{6h} structure of [30]annulene [27]. The transition state of the [30]annulene D_{6h} structure correctly switches to the D_{3h} structure in both the forward and reverse directions (i.e. the D_{3h} is the lowest energy structure of [30]annulene [27,49]). The D_{6h} - D_{3h} energy separation of [30]annulene at the B3LYP/6-31(d) and B3LYP/6-31(d,p) levels is 2.3 kcal/mol and 0.2 kcal/mol, respectively which are very small [49]. We have found an energy separation of 0.04 kcal/mol at the B3LYP/6-311+G(2d,p) level of theory. Due to this small energy separation, use of any of the two structures do not significantly affect the computed parameters. The imaginary frequencies for the different structures of [12]-, [18]-, and [30]annulenes in various functionals are listed in the supporting information (Tables S1- S5).

The ^{1}H NMR chemical shifts for the inner and outer protons for all the optimized [n]annulenes in the gas [$\delta_x^{(g)}$] and solution phase [$\delta_x^{(s)}$] where, x = i (inner) and o (outer); g = gas phase; s=

solvent phase; have been tabulated in Table 2. The inner and outer proton chemical shifts of the [12]annulene C_1 structure in THF are $\delta_i^{(THF)}$ = 8.864 ppm and $\delta_o^{(THF)}$ = 5.949 ppm, respectively; which are quite close to the experimental data (7.8 ppm and 5.9 ppm) in THF [46]. The calculated gas phase inner and outer proton chemical shifts are found to be $\delta_i^{(g)} =$ 8.637 ppm and $\delta_o^{(g)} = 5.856$ ppm which are close to the available reported theoretical data, 8.56 - 9.87 ppm and 6.01 to 6.22 ppm in the gas phase.

Note that, for the C_2 structure [18]annulene, the calculated values $\delta_i^{(g)}$ = -2.394 and $\delta_o^{(g)}$ = 8.877 ppm are also close to the available theoretical data in the gas phase, -2.7 to -2.9 (9 to 9.4) ppm [26]. From the computational results, we observe that the inner and outer proton chemical shifts of the C_2 structure of [18]annulene in THF and $CHCl_3$ are $\delta_i^{(THF)} =$ -2.634 ppm and $\delta_o^{(THF)} = 9.134$ ppm ; $\delta_i^{(CHCl_3)}$= 2.582 ppm and $\delta_o^{(CHCl_3)}$ = 9.090 ppm, respectively; which are close to the experimental data, -2.88 ppm and 9.25 ppm in THF [47], and -2.96 ppm and 9.17 ppm in $CDCl_3$ [48]. For the [30]annulene D_{6h} structure, the calculated gas phase inner and outer proton chemical shifts are found to be $\delta_i^{(g)} =$ -19.591 ppm and $\delta_o^{(g)} = 16.849$ ppm which are close to the available reported theoretical data, -20 ppm and 17.2 ppm in the gas phase [50] .

To quantify the SIS in terms of the computed chemical shift values, we first define a solvent induced shift value $\Delta\delta_x$ where $x = o, i$ represents the outer (o) and inner (i) protons of [n]annulenes. $\Delta\delta_x$ is defined mathematically as,

$$\Delta\delta_x = \delta_x^{(g)} - \delta_x \qquad (1)$$

Where $\delta_x^{(g)}$ is the chemical shift without solvent (gas phase) and δ_x is the chemical shift with solvent for the x^{ith} proton, and $\Delta\delta_x > 0$ and $\Delta\delta_x < 0$ indicate shielding and deshielding. The values of $\delta_x^{(g)}$ evaluated in this work and other reported values are indicated in Table 2. Using this definition, it is straightforward to evaluate the SIS values for the various solvents and we have tabulated these in Table 3. We plot these SIS values obtained from Table 3 as a function of the chosen solvent dielectric constants (ε) and show it in Fig. 2. From Table 3 and Fig. 2, we see that the SIS depends quite nonlinearly on the ε values for all the symmetries under consideration. We further observe that the outer protons in the annulenes show a complete deshielding effect in the SIS values ($\Delta\delta_x < 0$) which saturates at very high dielectric values.

Note that the behavior of the magnitude of change in SIS values is strikingly similar showing a sharp change at low polarities and saturation at higher polarities.

Let us now consider a specific case from Table 3, here the SIS values of the inner proton in the C_2 structure of [18]annulene in the highly polar solvent (DMSO) is $\Delta\delta_i$ = 0.453 ppm which is shielded from its n-hexane value of 0.059 ppm. The outer protons SIS value is $\Delta\delta_o$ = -0.368 ppm and is deshielded from the n-hexane value of -0.092 ppm. This indicates that the change in SIS (extent of deshielding) as a function of ε varies even within the same annulenic protons. This can also be visualized in Fig. 2, where each inner or outer protons response to the change in ε of the solvent is different from the other. To quantify the maximum deshielding response of an individual proton with respect to ε, we define a parameter, Δ_x, $x = i,o$ which is simply the ratio between the deshielded SIS value in DMSO (the deshielded value at which SIS has saturated, i.e., the maximum magnitude of SIS) and the deshielded SIS value in n-hexane for both inner and outer protons. This parameter, Δ_x is a measure of the maximum extent of change in the SIS values or maximum possible manifold of deshielding as the solvent polarity increases. For example, for the outer protons of the [18]annulene C_2 structure, Δ_o = - 0.368/-0.092 = 4. Likewise, for the same system, Δ_i = 0.453/0.059 = 7.677 ≈ 8. Thus, the inner protons are deshielded to eight-fold while the outer protons are deshielded to four-fold. We evaluated all the Δ_x values, which are tabulated in Table 3. For the inner protons of the asymmetric [12]annulene C_1 structure, $\Delta_i \approx 3$. For [30]annulene there is a three-fold deshielding for both the inner and outer protons. Interestingly, for both the inner and the outer protons of [12]- and [30]annulenes $\Delta_x \approx 3$, indicating that the maximum possible deshielding is three-fold. However, the shielding /deshielding observed in both the inner and outer protons of the C_2 structure of [18]annulene on the addition of solvents is greater than three. This observation lets us conclude that, the inner and outer protons of the annulenic systems respond differently to the reaction field. Specifically, the outer protons of all the annulenes are deshielded to a lesser extent than the inner protons.

Theoretical Corroboration

The nonlinear change observed in the SIS values of the annulenic protons can be understood using the Onsager's formalism of polarized electrical moments of solutes in liquid solvents or the reaction field theory. In accordance with this model, we assume that the annulene solute under consideration is a multipole immersed in a dielectric medium (the solvent) [12]. The

immersed multipolar annulene polarizes the dielectric medium, esp. the solvent neighborhood formed around the annulene. This polarization of the solvent environment forms a local internal electric field, (also called solvated field), a quantity that depends on the geometry and dimensions of the solvent neighborhood as well as the refractive index and polarizability of the solute (typically the gas phase value) [8]. This local cavity field alters the chemical shift in such a way that the SIS is given by the equation below [10],

$$\Delta\delta_x = -Af(\varepsilon) - Bf^2(\varepsilon). \qquad (2)$$

When $\Delta\delta_x > 0$ (shielding) and $\Delta\delta_x < 0$ (deshielding) occurs. In Eq. 2, $A\,f(\varepsilon)$ or $B\,f(\varepsilon)$ are referred to as the reaction field of the solute-solvent environment and is responsible for SIS by influencing the overall solvated system. $f(\varepsilon)$ is a nonlinear function of ε (called the dielectric function) [20], and is given by, under the assumption that the influence of the solvent reaction field

$$f(\varepsilon) = \frac{\varepsilon - 1}{\varepsilon/2 + 3/2} \qquad (3)$$

(in our case, the solvated annulene's activity site) is limited to the formation of a spherically solvated cavity (not to be confused with the annulenic cavity) around a disc shaped solute (which is annulene) with a microscopic quadrupole moment [20]. In Eq. 2, the quantity, A can be physically interpreted as the tendency of the multipole to be varied in the bond direction and is hence proportional to molecular polarizability. The quantity, B is related to the displacement of the multipole perpendicular to the resonant atom (i.e. hyperpolarizability) [9]. The proportionality constants, A and B although obtainable analytically in simple models, remain debatable and alternative theories of modeling such solvent effects exist in NMR spectroscopy [11]. Here, we treat A and B simply as system parameters whose values dictate the sign of SIS such that $A > B$ and $A > 0$ ($A < 0$) leads to deshielding (shielding). Physically, $A > 0$ ($A < 0$), represents the orientation the reaction field i.e., directed towards (away) from the proton leading to deshielding (shielding). Within the reaction field formalism, in a variety of studies, it has been reported that the dependence of $\Delta\delta_x$ on $f(\varepsilon)$ is linear (i.e. $A >> B$) and the effects due to second order terms is negligible since the magnitude of the solvated field is reported to be very small in comparison to the dielectric function at low values of solvent polarities [8,10,20]. In order to understand the quantitative change of the curves in Fig. 2, we simply assume A and B to be solvent and system dependent parameters and use the quadrupolar definition of $f(\varepsilon)$ in Eq. 2. We fit Eq. 2, utilizing the data given in Table 3 and by defining the fit variable to be f

(ε) = (ε -1)/(ε/2+3/2). The fit parameters are tabulated in Table 4 along with the usual error parameters (coefficient of determination, R^2 and root mean square error, *RMSE*). To quantify the extent of nonlinearity of SIS in $f(\varepsilon)$, we also tabulate the ratio, *A*:*B* for each of the annulenic protons.

The curve fitting technique reveals a complete linear dependency of outer annulenic protons of [12]- and [30]annulenes, since $|A| >> |B|$, (see Table 4) and each proton under the different symmetry groups have different slopes. In case of the low symmetric annulenes, i.e. for outer protons of the [12]annulene C_1 structure, $\Delta\delta_o < 0$, $|A| > 0$, and $|A| >> |B|$, which leads to a linear deshielding on the SIS (Fig. 3). Such linear dependencies are quite common in the literature [2,10,13]. For the inner protons, where $\Delta\delta_i < 0$, $|A| > 0$, and $|A|>|B|$. which results in a linear deshielding on SIS. A similar interference can be drawn for the [30]annulene D_{6h} structure, where, $\Delta\delta_o < 0$, $|A| > 0$, and $|A| >> |B|$ and results in linear deshielding for the outer protons. For the inner protons, $\Delta\delta_i < 0$, $|A| > 0$, and $|A| >|B|$, leads to a linear deshielding on SIS. From Table 4, we have observed $\Delta\delta_i > 0$, $|A| > 0$, and $|A|<<|B|$ for the inner protons of [18]annulene C_2 structure, demonstrating a nonlinear shielding as stated by Eq. 2. For the outer protons of the [18]annulene C_2 structure we have observed $\Delta\delta_o < 0$, $|A| > 0$ and $|A|\approx|B|$, showing a nonlinear deshielding on the SIS values as a function of the dielectric constants (Table 4, and Fig. 3). The graphical representations are shown in Fig. 3, and the blue curves of Fig. 3 show a nonlinear dependency for both the inner and outer protons for the [18]annulene C_2 structure.

For the inner protons of [12]- and [30]annulenes, we find that the nonlinear term, *B* is not very small in comparison to the linear term *A* (from Table 4, $|A|\approx|B|$). It has been reported that the term *B* gains importance only when solvent polarity is very high [9,20]. However, we see that within the same aromatic annulene, the inner (outer) protons behave nonlinearly (linearly) with the solvents polarity. The above-mentioned nonlinear dependency of the deshielded SIS values on the dielectric function for a different set of protons within the same molecule, to the best of our knowledge, is the first reported case. Since a general microscopic theory of SIS under arbitrary solvent and solute conditions is currently lacking [2], the specific origin of such nonlinearities within the same molecule cannot be ascertained and needs further study. Currently, we can only rationalize the reason based on the following arguments:

We consider the hyperpolarizability vector ($\vec{H}$) and the polarization vector ($\vec{P}$) to be oriented along the x-axis and y-axis respectively. Depending on the orientation of the reaction field vector ($\vec{R}$) with the $\vec{H}$ and $\vec{P}$, we can explain the SIS behaviors as per the following cases,

For the case of [30]annulene, the D_{6h} structure of [30]annulene is a large symmetric molecule with a significant inner ring cavity. Overall reaction field of the outer protons is oriented parallelly to the y-axis and hence $\vec{P}$ is influenced by $\vec{R}$. Thus, the angle between $\vec{R}$ and $\vec{P}$ which is denoted as θ_j becomes zero (Fig. 4e and Fig. 4f) and the resulting $\vec{R}$ is not influenced $\vec{H}$, being perpendicular to y-axis. Hence, the term *"A"* (Eq. 2) dominates, resulting in linear dependence of the SIS values with the solvent dielectrics and contribution from the *"B"* term is negligible (Table 4). This leads to the linear dependency of both the inner and outer protons with the solvent dielectric constants (Fig. 3a and Fig. 3b). For the case of [12]annulene, the [12]annulene C_1 geometry has a puckered structure. This puckered structure makes the individual bond dipole moment vectors to orient themselves in different directions randomly, resulting in $\vec{P}$ parrel to $\vec{R}$ and $\vec{P}$ perpendicular to $\vec{H}$ (Fig. 3a, Fig. 3b, Fig. 4a, and Fig. 4b,). For the case of [18]annulene, the net bond dipole moment vectors of the outer protons of the [18]annulene C_2 structure are oriented in between the y and z-axes. This makes the reaction field vector to orient in between these two axes leading the contribution of both $\vec{P}$ and $\vec{H}$on $\vec{R}$. Hence, $\vec{R}$ makes an angle with $\vec{P}$ ($\theta_j \neq 0^o$) (Fig. 4c and Fig. 4d), which results in the appearance of the nonlinear term *"B"* on $\vec{R}$ (Table 4, Fig. 3a and Fig. 3b).

On the other hand, owing to the small ring cavity of [18]annulene a local electric field is generated, which gives an extra contribution to the solvent reaction field ($\vec{R}$) for the inner protons along z-direction. This is taken care of by introducing the term "*C*", which accounts for the anisotropic environment inside the annulenic ring cavity with a new inner reaction field as given by Eq. 3 and shown in the inset (Table 4).

$$\Delta\delta_x = -Af(\varepsilon) - Bf^2(\varepsilon) - Cf^3(\varepsilon) \qquad (3)$$

This term "*C*" is also responsible for the nonlinear dependence of SIS on the solvent dielectrics (Fig. 3a). The term "*C"* signifies the presence of the overall reaction field in three axes (x, y and z) as shown in Fig. 4d.

5 Conclusions

We study the DFT computed ^{1}H NMR chemical shifts of the several structures of [n]annulenes [i.e., n = 12 (C_1), 18 (C_2), and 30 (D_{6h})] as a function of dielectric constants (ε) in 15 different solvents and results are further corroborated with the reaction field theory. It is observed that for each annulene, proton chemical shifts in presence of solvents show linear and nonlinear deshielding/shielding effect with respect to the solvent dielectrics. The inner and outer protons of the [12]annulene C_1 structure and [30]annulene D_{6h} structure exhibit the expected linear deshielding is predicted by the reaction field theory. The directions of the polarizability ($\vec{P}$), solvent reaction field ($\vec{R}$), and dipole moment ($\vec{\mu}$) of the [30]annulene D_{6h} structure are parallel to each other, resulting in an angle of 0º. The inner/outer protons of the [18]annulene C_2 structure exhibit nonlinear shielding/deshielding with the solvent dielectrics. This is because the hyperpolarizability ($\vec{H}$) arises and makes an angle of 45º between the directions of the polarizability/solvent reaction field and the dipole moment of the annulene. The asymmetry term "*C*" is also responsible for the nonlinear shielding of the inner protons of the [18]annulene C_2 structure. The hyperpolarizability term is nullified in the [12]annulene C_1 structure. The maximum extent of deshielding for the [12]annulene C_1 structure and [30]annulene D_{6h} structure are observed to be three-fold for both the inner and outer protons. The maximum extent of deshielding for the [18]annulene C_2 structure, is quantified to be higher than three-fold.

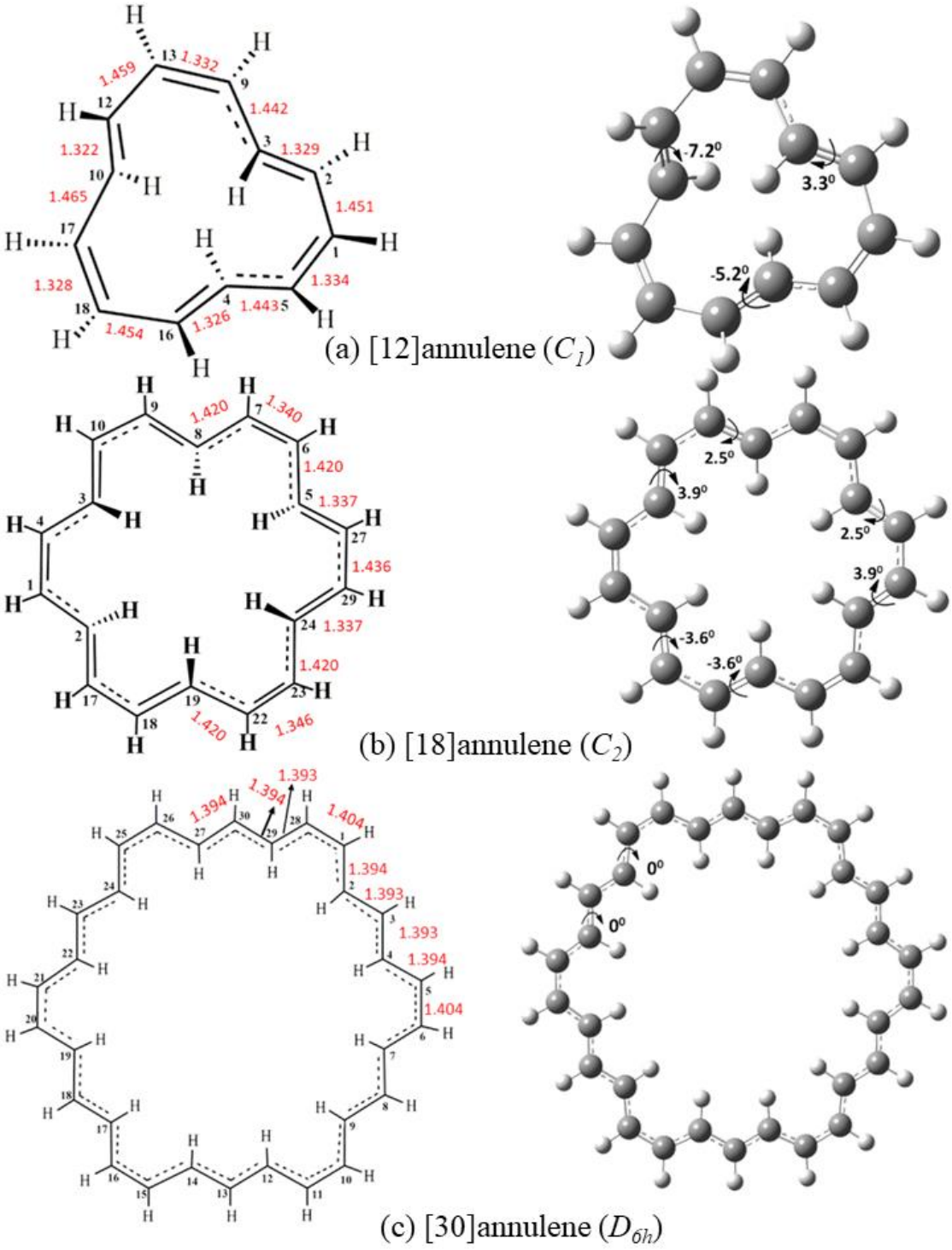

Fig. 1 (a) Manually drawn line structures and DFT optimized ball and bond type 3D structures of (a) the [12]annulene C_1 (b) the [18]annulene C_2 (c) the [30]annulene D_{6h} in THF. The bond distances (Å) and CCCH (inner hydrogen) dihedral angles (degree) are marked in the DFT optimized structures. The CCCH dihedral angles are centered on the double bonds. The [30]annulene D_{6h} structure has a dihedral angle of 0º for all the CCCH bonds.

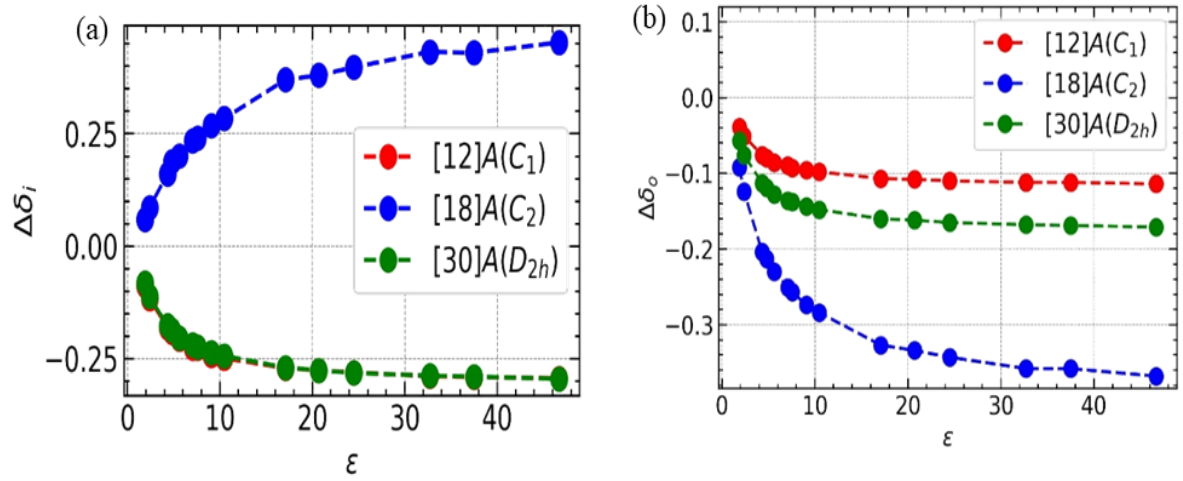

Fig. 2 SIS values for (a) inner and (b) outer protons of [n]annulenes plotted as a function of the dielectric constants of the solvents tabulated in Table 3. Dots represent computationally obtained results and dashed curves are interpolated results.

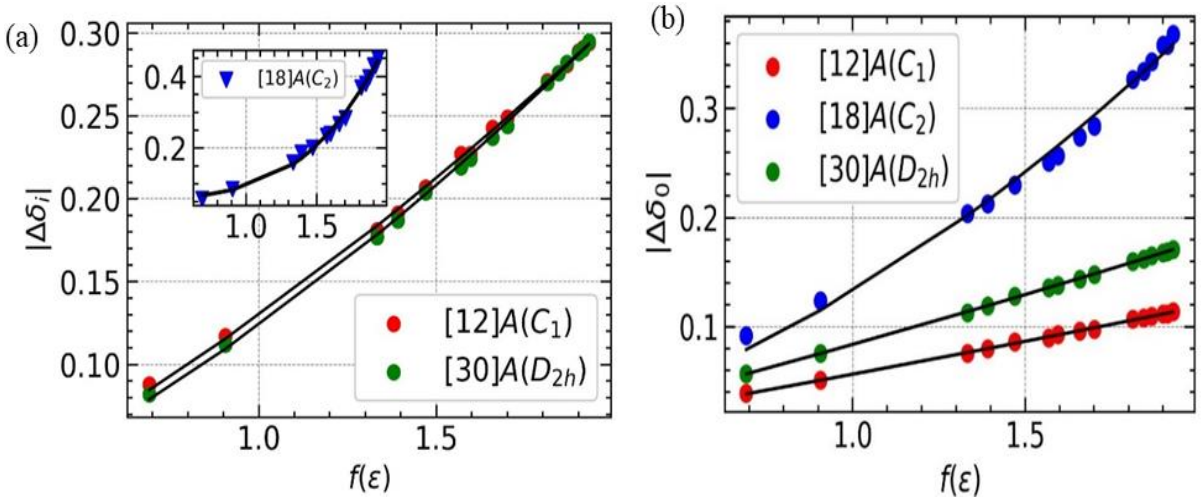

Fig. 3 Dependence of the absolute magnitude of the SIS values for the (a) inner and (b) outer protons of [n]annulenes (n = 12,18,30) as a function of the dielectric constant (polarity function). Dots are DFT results and the continuous curves are obtained via fitting of the DFT results using Eq. 2 with the quadrupolar dielectric function, $f(\varepsilon) = (\varepsilon - 1)/(\varepsilon/2 + 13)$. Note that we have shown only the magnitude of SIS for brevity. The actual sign of the slopes is obtained from Table 4. The blue curves on both the right- and left-hand sides indicate the nonlinear dependence of the inner and outer protons of [18]annulene C_2 structure, while the remaining curves depict the linear dependence with SIS.

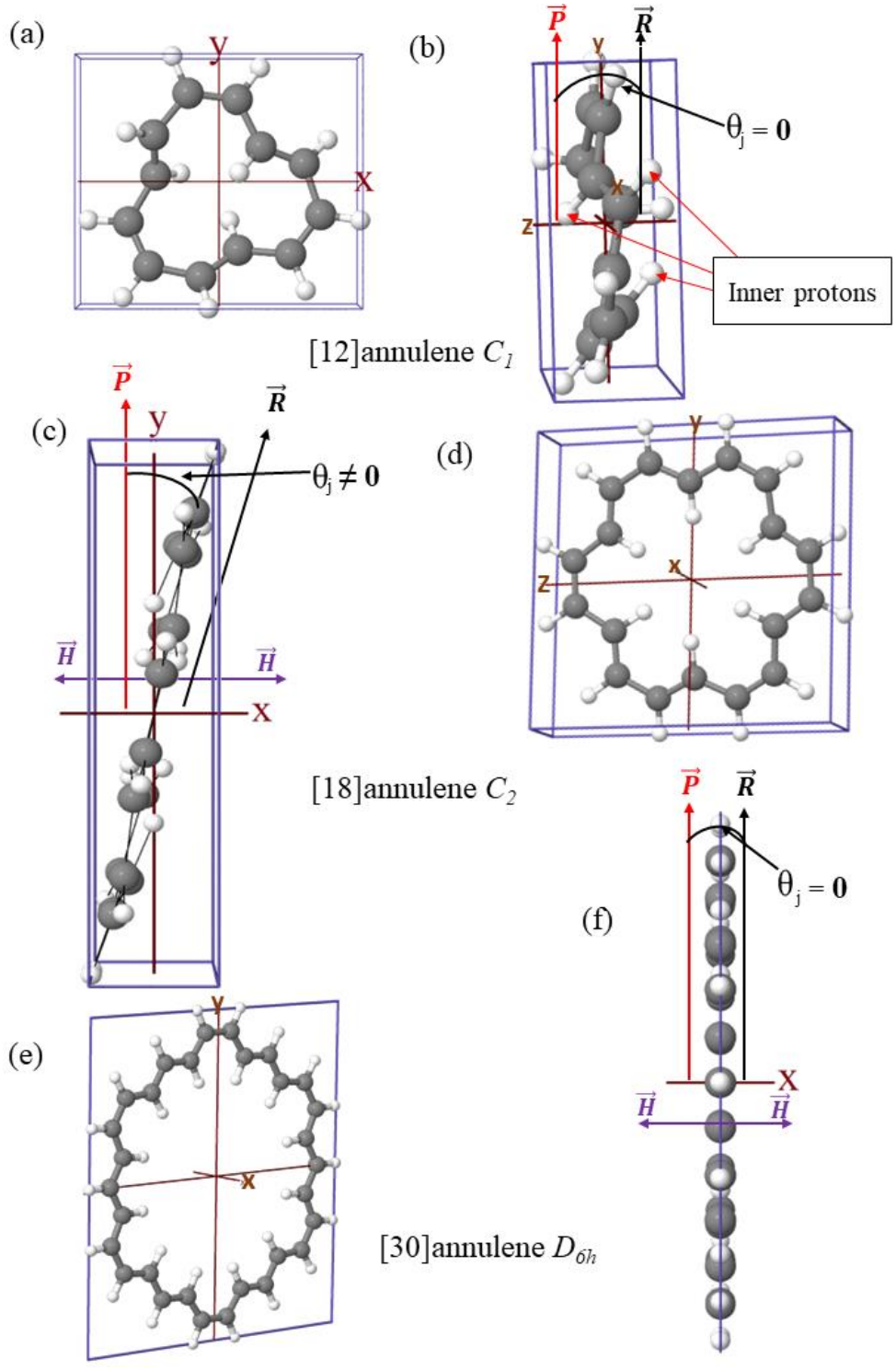

Fig. 4 The directions of the polarizability of annulene and the solvent reaction field are shown along the y-axis. Whereas, the hyperpolarizability is perpendicular to the y-axis. These vectors are depicted in the DFT optimized ball and bond type 3D structures of (a) and (b) [12]annulene C_1 ; (c) and (d) [18]annulene C_2; (e) and (f) [30]annulene D_{6h}. The $\vec{P}$, $\vec{H}$, $\vec{R}$ and θ_j are

shorthand notations for the polarizability, hyperpolarizability, overall solvent reaction field vectors, and angle between the polarization vector and the reaction field vector respectively.

Table 1 Relative energies (Hartree) and the number of imaginary frequencies of [n]annulenes (n = 12,18 and 30) in the gas phase and in various solvents. All energies are given relative to the gas phase. rel E = relative energy; NI = number of imaginary frequencies.

	[12]annulene (C_1)B3LYP		[18]annulene (C_2) B3LYP		[30]annulene (D_{6h})B3LYP	
	rel E (Hartree)	NI	rel E (Hartree)	NI	rel E (Hartree)	NI
Gas Phase	0	0	0	0	0	1
n- hexane	0.00134	0	0.00277	0	0.00463	1
Toluene	0.00177	0	0.00370	0	0.00617	1
Diethyl ether	0.00264	0	0.00571	0	0.00941	1
Chloroform	0.00277	0	0.00603	0	0.00990	1
Chlorobenzene	0.00298	0	0.00653	0	0.01071	1
Aniline	0.00317	0	0.00699	0	0.01142	1
THF	0.00323	0	0.00716	0	0.01167	1
Dichloromethane	0.00338	0	0.00754	0	0.01224	1
Dichloroethane	0.00346	0	0.00777	0	0.01309	1
1-butanol	0.00375	0	0.00857	0	0.01372	1
Acetone	0.00381	0	0.00874	0	0.01398	1
Ethanol	0.00387	0	0.00892	0	0.01423	1
Methanol	0.00395	0	0.00914	0	0.01452	1
Acetonitrile	0.00397	0	0.00919	0	0.01460	1
DMSO	0.00402	0	0.00935	0	0.01481	1

Table 2 GIAO based proton NMR chemical shifts for [n]annulene, (n =12, 18 and 30) computed at different optimized geometries in various solvents (1-15). The ^{1}H NMR chemical

shifts are calculated relative to TMS (computed proton shielding of TMS is 31.974 ppm in the gas phase). Available experimental and other reported values are also provided.

	[12]annulene (C_1)		[18]annulene (C_2)		[30]annulene (D_{6h})	
	δ_i (ppm)	δ_o(ppm)	δ_i(ppm)	δ_o (ppm)	δ_i (ppm)	δ_o (ppm)
Gas phase ($\delta_x^{(g)}$)	8.637	5.856	-2.394	8.877	-19.591	16.849
n- hexane	8.725	5.895	-2.453	8.969	-19.509	16.907
Toluene	8.754	5.907	-2.480	9.001	-19.479	16.926
Diethylether	8.818	5.932	-2.555	9.081	-19.414	16.963
Chloroform	8.828	5.936	-2.582	9.090	-19.404	16.969
Chlorobenzene	8.844	5.942	-2.595	9.107	-19.387	16.978
Aniline	8.864	5.946	-2.628	9.128	-19.372	16.985
THF	8.864	5.949	-2.634	9.134	-19.367	16.988
Dichloromethane	8.880	5.952	-2.662	9.151	-19.354	16.994
Dichloroethane	8.886	5.954	-2.678	9.161	-19.347	16.998
1-butanol	8.908	5.963	-2.764	9.204	-19.321	17.010
Acetone	8.913	5.964	-2.774	9.211	-19.315	17.012
Ethanol	8.918	5.966	-2.792	9.220	-19.309	17.015
Methanol	8.926	5.968	-2.826	9.235	-19.303	17.018
Acetonitrile	8.928	5.968	-2.824	9.235	-19.301	17.019
DMSO	8.931	5.970	-2.847	9.245	-19.296	17.021
Other reported values [26,46,50]	8.56 - 9.87	6.01 to 6.22	-2.7 to -2.9	9 to 9.4	-20	17.2
Experimental [46-48]	7.8 (-170^{0}C)	5.9 (-170^{0}C)	-2.88 (-60^{0}C)	9.25 (-60^{0}C)		

Table 3 Calculated $\Delta\delta_x$ (ppm, $x = i, o$) of [n]annulenes (n = 12, 18 and 30) structures using Eq. 1. The symmetries are shown in brackets. The last row consists of the maximum manifold of the extent of SIS for the inner and outer protons of each structure. Note that three-fold increase is common to both the inner and outer protons of [12]- and [30]annulenes. The dielectric constants (ε) values for the solvents are taken at $25^{\circ}C$.

	[12]annulene (C_1)		[18]annulene (C_2)		[30]annulene (D_{6h})	
Solvent, ε	$\Delta\delta_i$	$\Delta\delta_o$	$\Delta\delta_i$	$\Delta\delta_o$	$\Delta\delta_i$	$\Delta\delta_o$
n-hexane, 1.88	-0.088	-0.039	0.059	-0.092	-0.082	-0.057
Toluene, 2.38	-0.117	-0.051	0.086	-0.124	-0.112	-0.076
Diethyl ether, 4.33	-0.181	-0.076	0.161	-0.204	-0.177	-0.113
Chloroform, 4.81	-0.191	-0.080	0.188	-0.213	-0.187	-0.119
Chlorobenzene, 5.62	-0.207	-0.086	0.201	-0.230	-0.204	-0.128
Aniline, 7.06	-0.227	-0.090	0.234	-0.251	-0.219	-0.136
THF, 7.58	-0.227	-0.093	0.240	-0.257	-0.224	-0.138
Dichloromethane, 9.08	-0.243	-0.096	0.268	-0.274	-0.237	-0.144
Dichloroethane, 10.46	-0.249	-0.098	0.284	-0.284	-0.244	-0.148
1-butanol, 17.09	-0.271	-0.107	0.370	-0.327	-0.270	-0.160
Acetone, 20.07	-0.276	-0.108	0.380	-0.334	-0.276	-0.162
Ethanol, 24.5	-0.281	-0.110	0.398	-0.343	-0.282	-0.165
Methanol, 32.7	-0.289	-0.112	0.432	-0.358	-0.288	-0.168
Acetonitrile, 37.5	-0.291	-0.112	0.430	-0.358	-0.290	-0.169
DMSO, 46.68	-0.294	-0.114	0.453	-0.368	-0.295	-0.171
Δ_x	3	3	8	4	3	3

Table 4 Fit parameters of *A* and *B* obtained by fitting Eq. 2 with the SIS data provided in Table 3. *RSE = Residual sum of errors.

Annulene		Inner H	Outer H
[12]annulene (C_1)	*A, B*	-0.1058, -0.0239	-0.0540, -0.0025
	R^2, *RMSE*	0.997, 0.0017	0.999, 0.0006
	A : B,RSE	4:1,0.00132	21:1,0.00016
[18]annulene (C_2)	*A, B, C*	-0.1977, 0.2354, -0.239	-0.0748, -0.0576, 0
	R^2, *RMSE*	0.892, 0.008	0.991, 0.0071
	A : B: C,RSE	1:1:1, 0.0214	1:1:0, 0.0066
[30]annulene (D_{6h})	*A, B*	-0.0931, -0.0304	-0.0787, -0.0050
	R^2, *RMSE*	0.995, 0.0017	0.999, 0.0005
	A : B,RSE	3:1,0.0015	15:1,0.0001

References

[1] A. Konopacka, Z. Pawełka, J. Phy. Org. Chem. 18 (2005) 1190-1195.
[2] T. Welton, C. Reichardt, Solvents and solvent effects in organic chemistry, third ed. , John Wiley & Sons, 2011.
[3] P. Laszlo, E.M. Engler, J. Am. Chem. Soc. 93 (1971) 1317-1327.
[4] F.H.A. Rummens, R.H. Krystynak, J. Am. Chem. Soc. 94 (1972) 6914-6921.
[5] M. Hashimoto, K. Sakata, Anal. Sci. 11 (1995) 631-635.
[6] K.E. Wilzbach, J. Am. Chem. Soc. 79 (1957) 1013-1013.
[7] A. Brzyska, P. Borowski, K. Woliński, New J. Chem. 39 (2015) 9627-9640.
[8] A.D. Buckingham, T. Schaefer, W.G. Schneider, Chem. Phys. 32 (1960) 1227-1233.
[9] A.B. Sahakyan, Chem. Phys. Lett. 547 (2012) 66-72.
[10] J. Homer, Appl. Spectrosc. Rev. 9 (1975) 1-132.
[11] M. Dračínský, P. Bouř, J. Chem. Theory Comput. 6 (2010) 288-299.
[12] L. Onsager, J. Am. Chem. Soc. 58 (1936) 1486-1493.
[13] U. Holzgrabe, Prog. Nucl. Magn. Reson. Spectrosc. 57 (2010) 229-240.
[14] C. Lin, J. Skufca, R.E. Partch, BMC Chem. 14 (2020) 1-10.
[15] P.R. Young, R.C. Bogseth, E.G. Rietz, J. Am. Chem. Soc. 102 (1980) 6268-6271.
[16] P.E.M. Allen, B.O. Bateup, Eur. Polym. J. 9 (1973) 1283-1288.
[17] T. Hayashi, N. Mataga, T. Umemoto, Y. Sakata, S. Misumi, J. Phys. Chem. 81 (1977) 424-429.
[18] S. Masaki, T. Okada, N. Mataga, Y. Sakata, S. Misumi, Bull. Chem. Soc. Jpn. 49 (1976) 1277-1283.
[19] R.G. Wilson, J.H. Bowie, D.H. Williams, Tetrahedron 24 (1968) 1407-1414.
[20] P. Diehl, R. Freeman, Mol. Phys. 4 (1961) 39-47.
[21] N.K. Janjua, R. Qureshi, S. Ahmed, Y. K.A., M. Muhammad, S.M. Sadiq, R. Iqbal, Mol. Phys. 919 (2009) 321-324.
[22] E. Kang, H.R. Park, J. Yoon, H.Y. Yu, S.K. Chang, B. Kim, K. Choi, S. Ahn, Michrochem. J. 138 (2018) 395-400.
[23] T. Beyer, C. Schollmayer, U. Holzgrabe, J. Pharm. Biomed. Anal. 52 (2010) 51-58.
[24] F. Sondheimer, R. Wolovsky, Y. Amiel, J. Am. Chem. Soc. 84 (1962) 274-284.
[25] R.C. Haddon, Chem. Phys. Lett. 70 (1980) 210-212.
[26] C.S. Wannere, K.W. Sattelmeyer, H.F. Schaefer III, P.v.R. Schleyer, Angew. Chem. Int. Ed. Engl. 43 (2004) 4200-4206.
[27] C.H. Choi, M. Kertesz, Chem. Phys. 108 (1998) 6681-6688.
[28] T. Helgaker, M. Jaszunski, K. Ruud, Chem. Rev. 99 (1999) 293-352.
[29] A.A. Auer, J. Gauss, J.F. Stanton, Chem. Phys. 118 (2003) 10407-10417.
[30] T.A. Ruden, K. Ruud, Ro-vibrational corrections to NMR parameters, Calculation of NMR and EPR parameters (Theory and Applications), WILEY-VCH Verlag GmbH & Co. KGaA, Weinheim, 2004,pp. 153-173.
[31] K. Jackowski, M. Jaszuński, Gas Phase NMR, Royal Society of Chemistry 2016.
[32] E.E. Kwan, R. Liu, J. Chem.Theory Comput. 11 (2015) 5083-5089.
[33] D.B. Chesnut, Chem. Phys. 214 (1997) 73-79.
[34] Y. Liu, J. Saurí, E. Mevers, M.W. Peczuh, H. Hiemstra, J. Clardy, G.E. Martin, R.T. Williamson, Science 356 (2017) 5349-5356.

[35] G.V. Da Silva, Á.C. Neto, Tetrahedron 61 (2005) 7763-7767.
[36] M.W. Lodewyk, M.R. Siebert, D.J. Tantillo, Chem. Rev. 112 (2012) 1839-1862.
[37] J. Lee, L.D. Seymour, A.J. Pell, S.E. Dutton, C.P. Grey, Phys. Chem. Chem. Phys. 19 (2017) 613-625.
[38] L.B. Krivdin, Magn. Reson. Chem. 58 (2020) 5-14.
[39] A.C. Tsipis, Coord. Chem. Rev. 272 (2014) 1-29.
[40] P. Hodgkinson, Prog. Nucl. Magn. Reson. Spectrosc. 118 (2020) 10-53.
[41] D.L. Bryce, IUCrJ 4 (2017) 350-359.
[42] M.J. Frisch, G.W. Trucks, H.B. Schlegel, G.E. Scuseria, M.A. Robb, J.R. Cheeseman, G. Scalmani, V. Barone, G.A. Petersson, H. Nakatsuji, X. Li, M. Caricato, A.V. Marenich, J. loino, B.G. Janesko, R. Gomperts, B. Mennucci, H.P. Hratchian, J.V. Ortiz, A.F. Izmaylov, J.L. Sonnenberg, D. Williams-Young, F. Ding, F. Lipparini, F. Egidi, J. Goings, B. Peng, A. Petrone, T. Henderson, D. Ranasinghe, V.G. Zakrzewski, J. Gao, N. Rega, G. Zheng, W. Liang, M. Hada, M. Ehara, K. Toyota, R. Fukuda, J. Hasegawa, M. Ishida, T. Nakajima, Y. Honda, O. Kitao, H. Nakai, T. Vreven, K. Throssell, J.A. Montgomery, J.E. Peralta, F. Ogliaro, M.J. Bearpark, J.J. Heyd, E.N. Brothers, K.N. Kudin, V.N. Staroverov, T.A. Keith, R. Kobayashi, J. Normand, K. Raghavachari, A.P. Rendell, J.C. Burant, S.S. Iyengar, J. Tomasi, M. Cossi, J.M. Millam, M. Klene, C. Adamo, R. Cammi, J.W. Ochterski, R.L. Martin, K. Morokuma, O. Farkas, J.B. Foresman, D.J. Fox, Gaussian 16, Revision C.01 Gaussian, Inc. Wallingford CT (2016).
[43] J. Tomasi, B. Mennucci, R. Cammi, Chem. Rev. 105 (2005) 2999-3094.
[44] R. Cammi, B. Mennucci, J. Tomasi, Chem. Phys. 110 (1999) 7627-7638.
[45] R.E. Skyner, J.L. McDonagh, C.R. Groom, T. Van Mourik, J.B.O. Mitchell, Phys. Chem. Chem. Phys. 17 (2015) 6174-6191.
[46] C. Castro, W.L. Karney, C.M.H. Vu, S.E. Burkhardt, M.A. Valencia, J. Org. Chem. 70 (2005) 3602-3609.
[47] J.F.M. Oth, J. Pure Appl. Chem. 25 (1971) 573-622.
[48] C.D. Stevenson, T.L. Kurth, J. Am. Chem. Soc. 122 (2000) 722-723.
[49] K. Yoshizawa, M. Tachibana, T. Yamabe, J. Bull. Chem. Soc. Jpn. 72 (1999) 697-700.
[50] C.S. Wannere, P.v.R. Schleyer, Org. Lett. 5 (2003) 865-868.